Parametric Study of Thermal and Chemical Nonequilibrium Nozzle Flow

Philippe Sagnier* and Lionel Marraffa†
Office National d'Etudes et de Recherches Aérospatiales, Châtillon sous Bagneux, France

A numerical analysis of a thermochemical nonequilibrium inviscid nozzle flow was made for two types of wind tunnels. The first one was a French project of an arc jet wind tunnel. The second one was a generic wind tunnel, similar to a future European facility, with higher stagnation conditions than in the first wind tunnel. In the analysis, an equilibrium airflow is assumed up to the throat of the nozzles. Downstream, the calculation is carried out with a quasi-one-dimensional method, taking into account nonequilibrium thermochemistry, with possible vibration-dissociation coupling. There, the airflow is expanded quickly, and departure from equilibrium and then freezing are observed. Different models of chemical, electronic, and vibrational kinetics and different coupling models are studied. Their global influences are analyzed for one test condition for each wind tunnel. Futhermore, for the first nozzle, the computed frozen Mach number compares well with experimental results.

Nomenclature

Note: '(prime) is generally used for dimensional quantities. The nondimensionalization is made through a reference flow.

A = area
B_j = jth chemical species
Cp_j = specific heat of the jth species, $= C' p_j / R'$
c = number of chemical elements
E_j = average vibrational energy of dissociating molecule j
$E_j l$ = energy of lth electronic level, $= E' jl / R' T'^0$
ΔF_i^0 = change in the standard free energy of the ith reaction
G_j = average vibrational energy of recombining molecule
$g_j l$ = degeneracy of the lth electronic level
h = Planck's constant
h_j = enthalpy of the jth species, including heat of formation, $= h_j^f / RT'^0$
K_i = equilibrium constant of the ith reaction
Kp_i = equilibrium constant of the ith reaction in terms of partial pressures
k = Boltzmann's constant
k_{fi}, k_{bi} = forward and backward reaction rate coefficient, respectively
M = gas mixture molecular weight, $= M' / M'^0$
Mf = frozen Mach number, $= U' (P/\rho \, \Delta\rho / \Delta P)^{0.5}$
m_j = number of electronic levels
m_j' = jth species molecular weight
N_j = number of vibrational levels
n_j = number of atoms per molecule
P = thermodynamic pressure, $= P' / \rho' U'^{0^2}$
Q_{ij} = mole production volumetric rate of the jth species in the ith reaction, $= Q_{ij}' M'^0 / \rho' U'^0$
R' = universal gas constant
s = number of species
T = translational temperature, $= T' / T'^0$
T_{Pj} = $(Tv_j \, T)^{0.5}$
Tm_j = $(Tv_j T)/(Tv_j - T)$
Tv_j = vibrational temperature
U = flow velocity, $= U' / U'^0$
Vj = nonpreferential vibration-dissociation coupling factor
x = abscissa along the nozzle axis
α_{jk} = number of atoms of the kth element in the jth species
β_{ij} = $\nu^*_{ij} - \nu_{ij}$
β_i = $\sum_{j=1}^{s} \beta_{ij}$
γ_j = concentration of the jth species, $= \gamma'_j M'^0$
ϵ_j = vibrational energy of the jth species, $= \epsilon'_j / R' T'^0$
θr_j = characteristic rotational temperature of the jth species
θv_j = characteristic vibrational temperature of the jth species
Λ = nondimensionalizing factor, $= U'^{0^2} M'^0 / R' T'^0$
μ_j^0 = chemical potential at standard pressure of the jth species, $= \mu_j'^0 / R' T'^0$
ν_{ij} = stoichiometric coefficient of the jth species in the first member of the ith reaction
ν^*_{ij} = stoichiometric coefficient of the jth species in the second member of the ith reaction
ρ = density, $= \rho' / \rho'^0$
τ_j = relaxation time of vibration of the jth species
ω_j = vibration frequency of the jth species

Subscripts and superscripts

i = ith reaction
j, α = jth or αth species
l = lth electronic level
v = vth vibrational level
0 = initial state or reference state
∞ = value at vibrational equilibrium
$'$ = dimensional quantities

Introduction

In conjunction with its projects for the HERMES space shuttle, Europe is involved in the design of new hypersonic wind-tunnel facilities. The stagnation conditions of such wind tunnels have to be high enough to simulate the re-entry real gas effects and to test the real gas calculation methods.

The Office National d'Etudes et de Recherches Aérospatiales (ONERA) has studied a project of hypersonic wind tunnels.[1,2] Air is heated through a plasma generator (power = 5 MW), and the flow is expanded through a nozzle with a

Received Aug. 24 1989; revision received Feb. 6, 1990.

*Research Scientist. Member AIAA.
†Research Scientist.

conical divergent (11.3 deg half angle). The nozzle length is about 25 cm and the throat area is 1 cm^2. The stagnation pressure is 50 bars and the normalized stagnation enthalpy (Hi/RT^0) is 100 (i.e., the stagnation temperature is about 4800 K). The frozen Mach number Mf is about 6 at the exit.

The stagnation conditions of the second facility are 600 bars for the pressure and 320 for normalized enthalpy (i.e., about 10,000 K for temperature). The nozzle length is about 200 cm and the throat are is 3.14 cm^2. The divergent part of the nozzle is a cone with a half angle of 10 deg.

The nonequilibrium zones of both nozzle flows were investigated with a quasi-one-dimensional method,[3-6] which is discussed later.

The purpose of the present study is to estimate the influences of thermochemical models on the calculation results. It is, therefore, a parametric study; unfortunately, it is not exhaustive due to the abundance of today's known models. Our goal is to show that the method easily allows an overview of the main phenomena present in a nozzle flow and can be used to find simplifications applicable to more involved two-dimensional or three-dimensional computations.

Numerical Method

The real gas flows fundamental equations might take into account the classical aspects of aerodynamics. Real gas phenomena have to be added: the chemical and thermodynamical states of the flow could be very different than for ideal gas flows. These effects must be modeled as well as possible. A steady one-dimensional code,[3] first designed for flow relaxation behind normal shock waves, has been extended for nozzle flows[5] (quasi-one-dimensional). It takes into account chemical and vibrational nonequilibrium kinetics (for molecules with a maximum of two atoms), with vibration-dissociation coupling, and electronic excitation (at translational temperature). The rotation of diatomic molecules is assumed to be in equilibrium with translation. Virial effects and transport properties are not accounted for. Ionization reactions can be included, but the free electrons have the same translational temperature as the other species.

The nondimensional governing equations are the following:

Continuity equation:

$$\frac{d\rho}{dx} = -\frac{\rho}{U}\frac{dU}{dx} - \frac{\rho}{A}\frac{dA}{dx} \tag{1}$$

Conservation equation of the jth chemical element:

$$\frac{d\gamma_j}{dx} = \frac{1}{\rho U}\sum_{i=1}^{r} Q_{ij} \qquad j = c+1,\ldots,s \tag{2}$$

Conservation equation of the kth chemical element:

$$\sum_{j=1}^{s} \alpha_{jk}\frac{d\gamma_j}{dx} = 0 \qquad k = 1,\ldots,c \tag{3}$$

Momentum equation:

$$\frac{dP}{dx} = -\rho U\frac{dU}{dx} \tag{4}$$

Energy equation:

$$\Lambda U\frac{dU}{dx} = -\sum_{\alpha=f+1}^{g}\gamma_\alpha(n_{\alpha-1})\frac{d\epsilon_\alpha}{dx} - \Lambda\frac{M}{\rho}\left(\frac{dP}{dx} - \frac{Pd\rho}{\rho dx}\right)$$

$$\sum_{\alpha=1}^{s}\gamma_\alpha Cp_\alpha - \sum_{\alpha=1}^{s}\sum_{j=1}^{s}\left(\frac{h_j}{s} - \Lambda\frac{M^2}{\rho}P\gamma_\alpha Cp_\alpha\right)\frac{d\gamma_j}{dx} \tag{5}$$

where f is the index of the first nonequilibrium vibrating species and g is the index of the last one.

Vibrational energy equation of the jth diatomic species:

$$\frac{d\epsilon_j}{dx} = \frac{S\epsilon_j}{U} \tag{6}$$

The system [Eqs. (1-6)] is first solved with respect to the space derivatives of the unknowns U, P, ρ, γ_j, and ϵl_j. These derivatives are then integrated with a fourth-order Runge-Kutta method.

The state equation, needed for closure of the system, gives the translational temperature:

$$T = MP/\rho \tag{7}$$

There are other relations, especially electronic and vibrational contribution, in Appendix A.

Let us describe the source terms Q_{ij} [Eq. (2)] and $S_{\epsilon j}$ [Eq. (6)]. Molecular exchanges are governed by collisions. When a collision occurs, the impinging atoms or molecules exchange their energy in different modes (translation, rotation, vibration). If the energy of the collisions is high enough, dissociations of multiatomic molecules are possible. Their results are modeled by the right sides of Eq. (2-6). When the frequency of these collisions is very high (equilibrium), the state of the gas depends only on local thermodynamic parameters (P, T, for example). If the frequency of the collisions is too low, the state of the gas depends on the flow history (nonequilibrium). The gas tries to reach equilibrium without ever achieving it. When the collisions become rare (i.e., low density and high velocity), no further exchanges between particles occur and the flow is frozen. Its thermochemical properties remain constant. These three states are characteristic of our nozzle flow examples: from the reservoir up to the throat, the expansion is slow enough for the flow to stay in a near-equilibrium state. In the throat region, where the expansion becomes faster, nonequilibrium occurs, and downstream, the flow freezes when low density and high velocity occur.

The right side of vibrational Eq. (6) is a function of the chosen vibrational model. This term takes into account the variations of vibrational energy due to two distinct phenomena. On the one hand, when a diatomic molecule is in a nonequilibrium vibrational state (i.e., its vibrational temperature is different from its translational temperature), it tends to relax to equilibrium through collisions with other particles along its trajectory. On the other hand, when two atoms recombine and yield a diatomic molecule, the vibrational energy of this molecule is often higher than the average vibrational energy. This can lead to an inversion of vibrational population. The same reasoning applies to dissociation. The more a molecule is vibrationally excited, the more easily it dissociates. That means also that dissociations deplete the higher vibrational levels and, therefore, decrease the average vibrational energy of the gas mixture.

The first phenomenon (vibrational relaxation to equilibrium) is modeled through a Landau-Teller law[7] with coefficients from Blackman.[8] The second phenomenon (vibration-dissociation coupling) is modeled by the nonpreferential model of Marrone.[3] Both are based on the harmonic oscillator, and their contribution corresponds to the source term $S\epsilon_j$. The coupling influences both dissociation and recombination rates through a coupling factor V_j. Here, V_j assumes an equal dissociation probability (nonpreferential) for each vibrational level in the case of a collision energetic enough for dissociation to occur. Note that the preferential model,[3] based on an anharmonic oscillator and favoring coupling between dissociation recombination and the highest levels of vibration, could be also implemented but has not been tested here.

For r chemical reactions using a set of s species, we have

$$\sum_{j=1}^{s} v_{ij}B_j <=> \sum_{j=1}^{s} v^*_{ij}B_j \qquad i = 1,\ldots,r \tag{8}$$

The production term in Eq. (2) writes

$$Q'_{ij} = (\nu^*_{ij} - \nu_{ij}) \left(k_{fi} \rho'^{\nu_i} \prod_{\alpha=1}^{s} \gamma_\alpha'^{\nu_{i\alpha}} - k_{bi}'^{\infty} \rho'^{\nu^*_i} \prod_{\alpha=1}^{s} \gamma_\alpha'^{\nu^*_{i\alpha}} \right) \quad (9)$$

with

$$\nu_i = \sum_{j=1}^{s} \nu_{ij} \text{ and } \nu^*_i = \sum_{j=1}^{s} \nu^*_{ij}$$

The real forward reaction rate (i.e., with vibration-dissociation nonpreferential coupling) writes

$$k'_{fi} = k'^{\infty}_{fi} \prod_{\alpha=1}^{s} V_j^{Aij} \quad (10)$$

with $A_{ij} = 1$ or 0 according to whether the ith reaction is affected by the coupling process.

The ratio between the constants k'^{∞}_{fi} and k'^{∞}_{bi} is given by

$$K'_i = \frac{k'^{\infty}_{fi}}{k'^{\infty}_{bi}} \quad (11)$$

where K'_i is the equilibrium constant depending on the chemical potentials (see Appendix A) and k'^{∞}_{ri} and k'^{∞}_{bi} are the forward and backward reaction constants, respectively, given in the literature under the modified Arrehenius law form:

$$k'^{\infty}_i = a_i T'^{b_i} \exp\left(\frac{-c_i}{T'}\right) \quad (12)$$

The V_j terms are introduced in Eq. (10) to take into account the influence of the vibrational excitation, assuming the harmonic osicllator model, on dissociations:

$$Vj = \frac{1}{N_j} \frac{1 - \exp(-N_j \Theta_{vj}/T_{mj})}{\exp(\Theta_{vj} T_{mj}) - 1} \frac{\exp(\Theta_{vj}/T_{vj}) - 1}{\exp(\Theta_{vj}/T_{vj}) - 1} \quad (13)$$

The source term $S\epsilon_j$ for the nonpreferential model writes

$$S\epsilon_j = \frac{\epsilon_j^{\infty} - \epsilon_j}{\tau_j} - \left(\frac{d\gamma_j}{dt}\right) f \frac{E_j(T, Tv_j) - \epsilon_j}{\gamma_j} + \left(\frac{d\gamma_j}{dt}\right) b \frac{G_j(T) - \epsilon_j}{\gamma_j} \quad (14)$$

where $(d\gamma j/dt)f$ and $(d\gamma j/dt)b$ are the production and vanishing terms of the diatomic species, respectively (see Appendix A for the expressions of $\epsilon_j\infty$ and T_{vj}). The terms $E_j(T, T_{vj})$ and $G_j(T)$ represent, respectively, the average vibrational energies of a dissociating molecule and of a molecule immediately after recombination:

$$E_j(T, T_{vj}) = \frac{\omega_j}{\exp(\omega_j/kTm_j) - 1} - \frac{N_j \omega_j}{\exp(N_j \omega_j/kTm_j) - 1} \quad (15)$$

$$G_j(T) = \frac{1}{2} \omega_j (N_j - 1) \quad (16)$$

$S_{\epsilon j}$ can be rewritten as

$$S_{\epsilon j} = \frac{\epsilon_j^{\infty} - \epsilon_j}{\tau_j} + \left[\frac{\Theta v_j}{\exp(\Theta v_j/Tm_j) - 1} - \frac{N_j \Theta v_j}{\exp(N_j \Theta v_j/Tm_j) - 1} - \epsilon j \right] \sum_{i=1}^{r} \frac{A_{ij} Q_{ij}}{\gamma_j \rho X_i} - \left[\frac{\Theta v_j}{2} (N_j - 1) - \epsilon_j \right] \sum_{i=1}^{r} \frac{A_{ij} Q_{ij} (1 - X_i)}{\gamma_j \rho X_i} \quad (17)$$

with

$$X_i = 1 - \frac{1}{K_i' V_j A_{ij}} \rho'^{\beta i} \prod_{\alpha=1}^{s} \gamma'^{\beta i\alpha}_{\alpha} \quad (18)$$

A simplified model (Park coupling model[18,19]), first designed for relaxing flows behind normal shock waves, has also been tried in this study. Park assumed an average temperature Tp_j that he used in the calculation of the dissociation reaction constants [Eq. (12)] instead of the translational temperature T. The vibrational energy source term $S_{\epsilon j}$ is thereby simplified:

$$S\epsilon_j = \frac{\epsilon_j^{\infty} - \epsilon_j}{\tau_j} \quad (19)$$

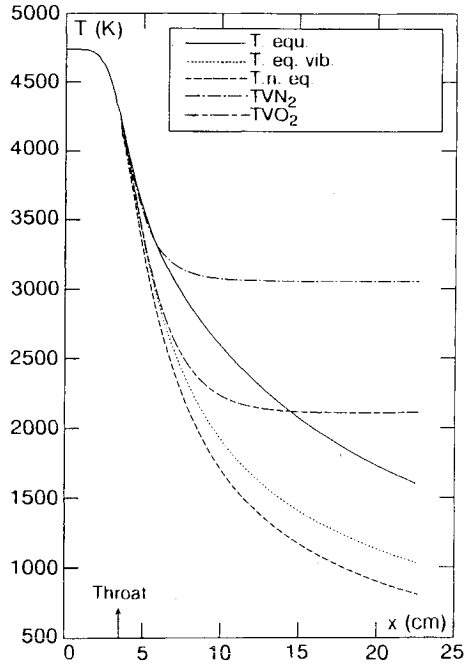

Fig. 1 Moss model: full equilibrium, vibrational equilibrium, and full nonequilibrium temperatures.

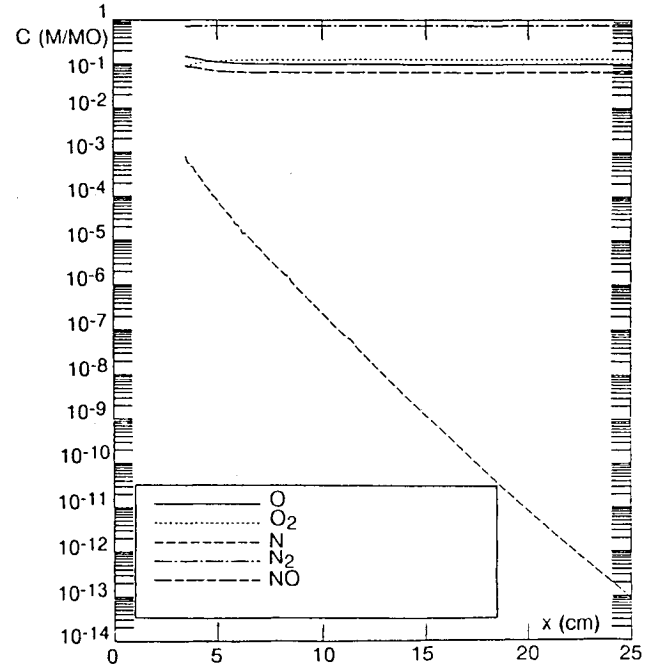

Fig. 2 Moss model: nonequilibrium species concentrations.

The characteristic vibrational relaxation times in Eqs. (14), (17), and (19) for O_2 and N_2 are given by the Landau-Teller expressions.

$$O_2: \quad \tau j\, P' = 16.18\ 10^{-4} \exp\left(\frac{101.44}{T'^{1/3}}\right) \tag{20}$$

$$N_2: \tau_j P' = 11.15\ 10^{-6}\, T'^{1/2} \exp\left(\frac{154}{T'^{1/3}}\right) \text{ in baryes seconds} \tag{21}$$

Chemical Models

The computation of a flow with chemical kinetics requires as realistic as possible a choice of reactive species and the appropriate reactions with their rate coefficients. In recent studies, these rates have been compared.[11] Their applications in inviscid flows behind shock waves[12] and in viscous flows including shock layer[13] and boundary layer[14–16] were demonstrated. Nevertheless, as far as we know, no such studies have been made for hypersonic nozzle flows. We restrict the study to a few classical chemical models with all or part of the following species: *O, N, O_2, N_2, NO, NO^+, O^+, N^+, O_2^+, N_2^+*, and the electrons *e*. Five sets of chemical models[10,17–20] have been used (for some of them, we have not selected ionization reactions). For simplicity, they will be called Moss, Gardiner, Evans-Schexnayder-Huber (ESH), Dunn-Kang (DK), and Park models. Their characteristics are detailed in Appendix B. The Moss model is chosen as the reference model

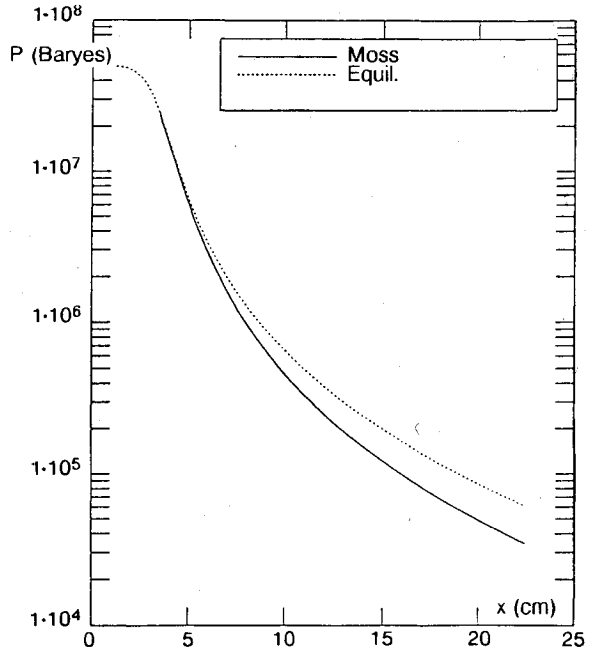

Fig. 3 Moss model: equilibrium and nonequilibrium pressure.

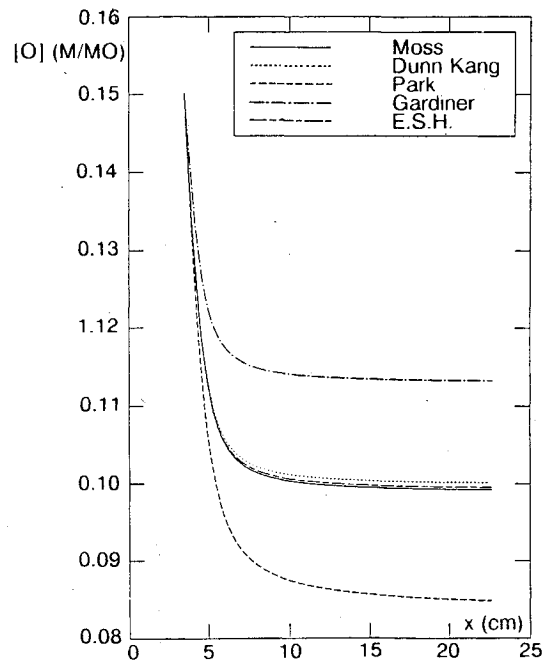

Fig. 5 Chemical model effects: [O].

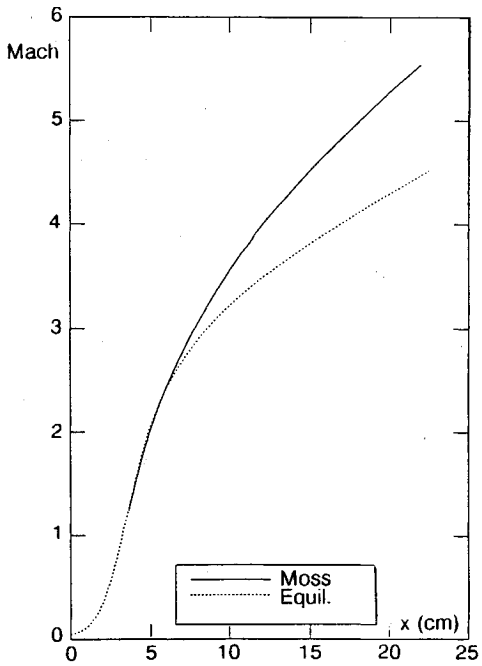

Fig. 4 Moss model: equilibrium and nonequilibrium frozen Mach number.

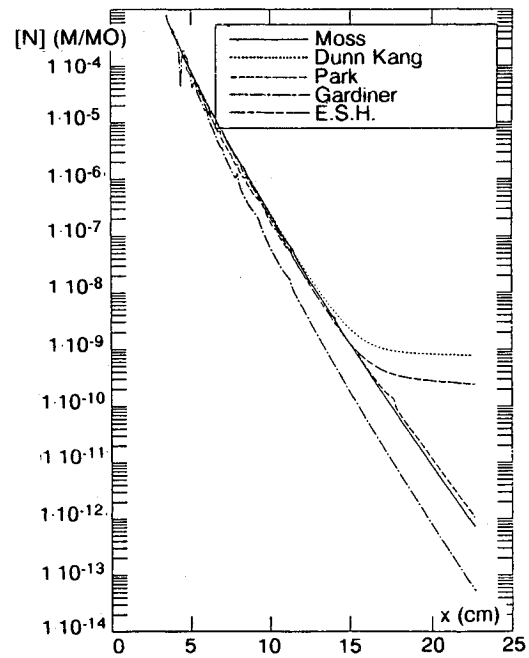

Fig. 6 Chemical model effects: [N].

for comparison for results. Ionization, when computed with the ESH and DK models, is weak in our nozzle flows. Thus, the results relative to the species concentrations exhibit only electrically neutral species. For comparison, we have also computed the nozzle flows at equilibrium with a tabulated Mollier diagram from Ref. 21. This diagram does not supply the concentrations of the species.

Analysis of the Results

ONERA Prototype

First, we establish a reference calculation case consisting of Moss chemistry, electronic excitation, nonequilibrium vibration of O_2 and N_2, and Marrone nonpreferential coupling. Then, we compare these results with those given by the other chemical sets. Influences of electronic excitation (with Moss chemistry) and of nonequilibrium vibration and the Marrone and Park coupling are also studied. In all of the cases, the results are presented as a function of the abscissa along the nozzle axis. Finally, a comparison with an experiment is presented for the frozen Mach number.

The code fails when trying to compute near equilibrium flow.[5,6] Therefore, the nonequilibrium computation is started with an equilibrium initialization 2 mm downstream of the throat (at $x = 3.5$ cm).

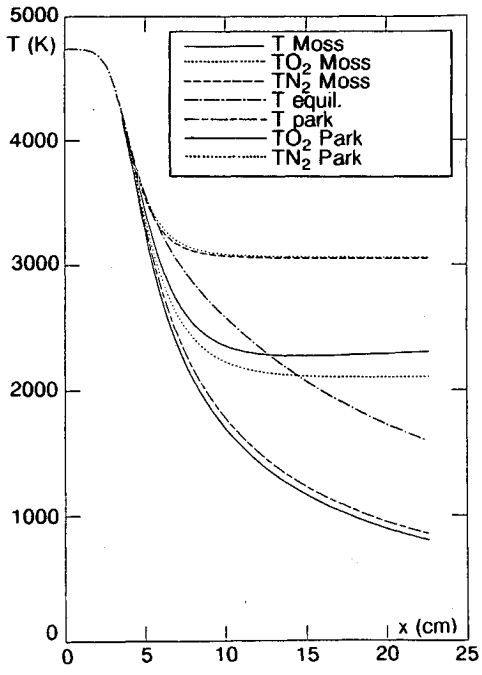

Fig. 7 Moss and Park chemical model effects: temperatures *T*, *Tv*O2, *Tv*N2, and equilibrium.

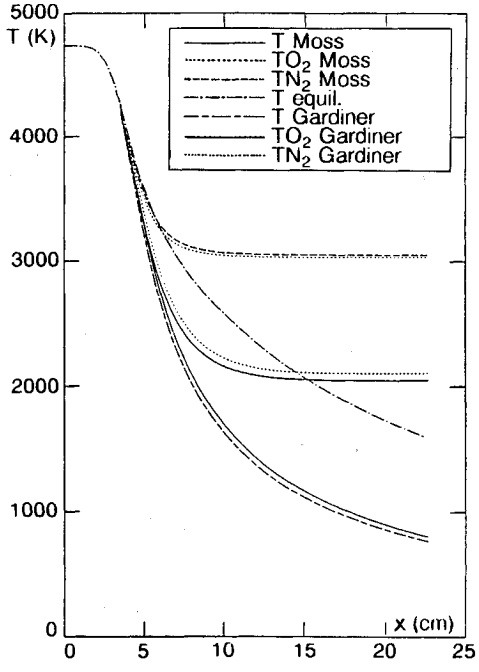

Fig. 8 Moss and Gardiner chemical model effects: temperatures *T*, *Tv*O2, *Tv*N2, and *T* equilibrium

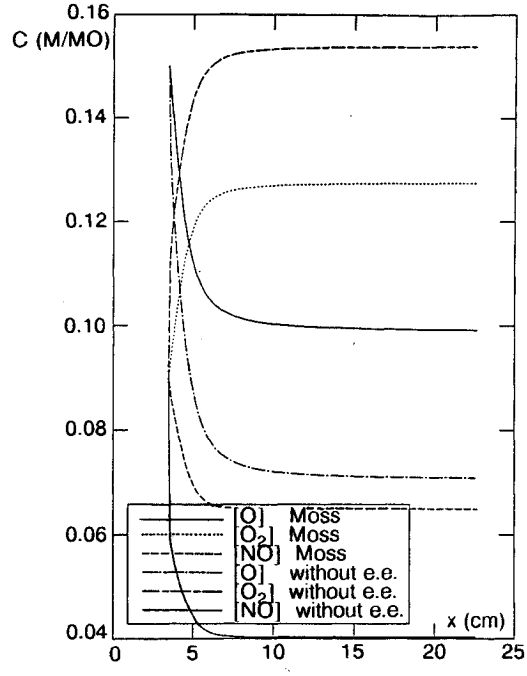

Fig. 9 Electronic excitation effects: species concentrations.

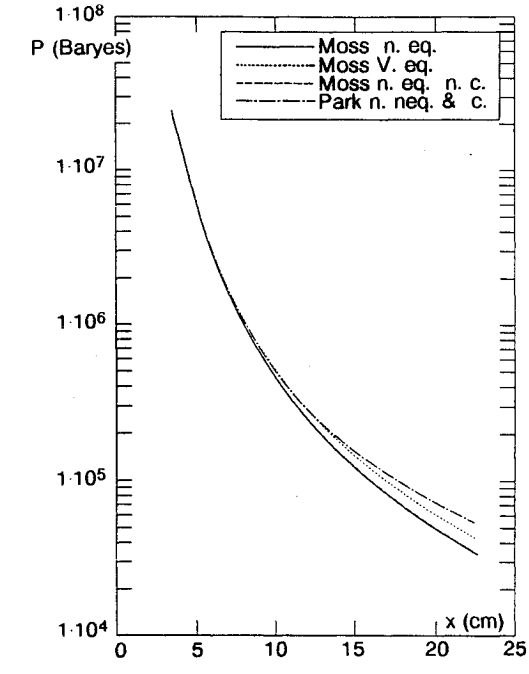

Fig. 10 Vibrational nonequilibrium and vibration-dissociation coupling effects: pressure.

Analysis of the Results for the Moss Model

In a hypersonic nozzle, it is interesting to know the flow evolution in terms of departure from equilibrium and freezing and, of course, its exit composition. Figure 1 shows the evolutions of several temperatures: equilibrium (T.equ.), translational nonequilibrium with vibrational equilibrium (T.eq. vib.), the same with vibrational nonequilibrium (T.n.eq.), and for the vibration of O_2 and N_2 (TVO2, TVN2). There are large differences between the translational temperatures: at the exit 1600 K for T.eq., 1000 K for T.eq.vib., and 800 K for T.n.eq. The nonequilibrium temperatures depart quickly from the equilibrium temperature, showing that nonequilibrium does exist upstream of the throat. The same remark can be made for the vibrational temperatures. Moreover, the freezing of

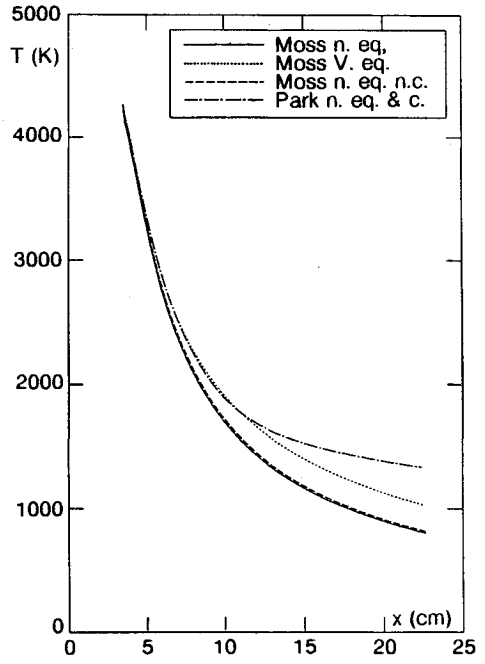

Fig. 11 Vibrational nonequilibrium and vibration-dissociation coupling effects: translational temperature.

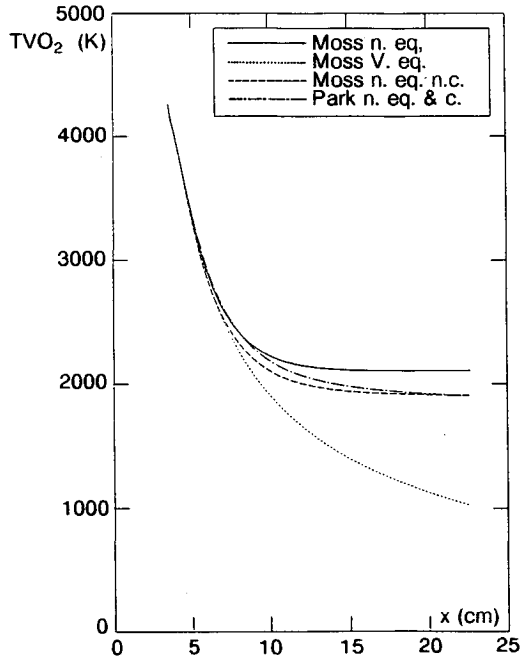

Fig. 12 Vibrational nonequilibrium and vibration-dissociation coupling effects: vibrational temperature of oxygen.

TVO2 and TVN2 can be observed at about 12 and 8 cm, respectively. This shows that the storage of frozen vibrational energy cannot be neglected and explains the differences between T.n.equ. and T.eq.vib. When comparing T.eq.vib. and T.equ., we can see the effect of nonequilibrium chemistry on the translational temperature. The molar concentrations of the species are presented in Fig. 2. The freezing of the main species is observed at about 7 cm, except for N, which recombines (but in negligible amounts) up to the exit due to the high rates of N_2 recombination reactions. Equilibrium and full nonequilibrium assumptions also have an influence on P (Fig. 3) (equilibrium pressure is about twice the nonequilibrium value at the exit) and on Mf (Fig. 4) (5.6 vs 4.6 for equilibrium at the exit). However, velocity and density remain almost the same in both assumptions due to the mass flow conservation (so we do not represent them). All of these results show that the flow is in thermal and chemical nonequilibrium in the divergent part of the nozzle.

Influence of the Chemistry

Globally, the results are weakly influenced by chemical models. The DK, ESH, and Moss models are almost overwhelmed. Therefore, we focus especially on the Moss, Gardiner, and Park models (and equilibrium). The model that is closest to equilibrium is Park's, the farthest one is Gardiner's.

Two general comparisons can be made. One concerns O molar concentrations ([O]) (Fig. 5). The small difference between the ESH, DK, and Moss models allows us to avoid plotting the corresponding curves in the following. The second concern [N] (Fig. 6) and shows late freezing for ESH and DK, which are the only models with ionization. Furthermore, for [N], Gardiner's model is much closer to equilibrium than Park's, but it is difficult to draw a conclusion for such a small amount of a species.

Figures 7 and 8 are relative to temperatures. Translational temperatures confirm the previous remarks about Park and Gardiner for their equilibrium proximity. However, the situation is reversed for vibrational temperatures. This is because, for Gardiner, for example, the chemical energy storage is high and so there is less energy available for vibration. That and the lower translational temperature for the Landau-Teller law imply lower frozen vibrational temperatures.

Influence of the Electronic Excitation

The code takes into account the contribution of electronic excitation. It is possible to switch it off to study its effects. It appears that this influence is negligible on aerodynamics, weak on temperatures and [N], but important on [O], [O_2] and [NO] (Fig. 9). Furthermore, as shown in Fig. 9, recombination rates are higher without electronic excitation. This leads to stability problems in the near equilibrium zone and, therefore, to a longer computational time because of shorter space step sizes.

Influence of Vibrational Nonequilibrium and Its Coupling with Chemistry

All the following cases take into account electronic excitation. We have tested Moss and Park chemical sets, each one with the nonpreferential coupling (Moss et al.) and the Park coupling (Park et al.); we have also tried combinations of these but the results are qualitatively the same. Moreover, we have also plotted results with Moss chemistry without coupling (Moss n.eq. n.c.) and with vibrational equilibrium (Moss V.eq. which with Moss n.eq. could represent a reference band). Results are presented for P (Fig. 10), T (Fig. 11), TvO2 (Fig. 12), TvN2 (Fig. 13), and [O] (Fig. 14). The first remark that can be made is the small influence of the nonpreferential coupling: the major effects are observed on the vibration of O_2 (Fig. 12) and N_2 (Fig. 13). The effect on TvO2 is more important than on TvN2 since O_2 chemistry is more active.

Park coupling gives rather different results, but only after a

certain distance. This is because the rates of dissociation and recombination are computed using a geometrical average of translational and vibrational temperatures. There is still freezing of vibration of N_2 and O_2 in the same way as for Moss et al. But since the vibrational temperature freezes at a rather high level, the average temperature remains quite high. This explains why no chemical freezing is observed in the plots of [O] (Fig. 14). Thus, the kinetics of recombination remain sufficiently rapid to prevent freezing. However, the decreasing translational temperature changes the equilibrium constant, especially toward the nozzle exit, producing more recombinations. This may explain why the slope changes in the plot of [O].

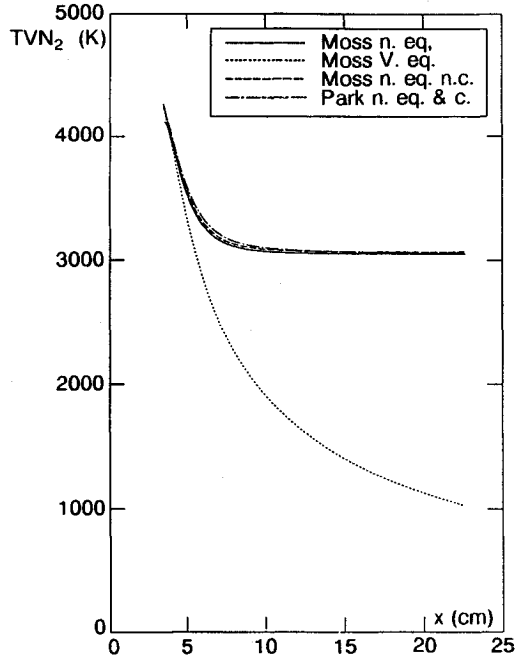

Fig. 13 Vibrational nonequilibrium and vibration-dissociation coupling effects: vibrational temperature of nitrogen.

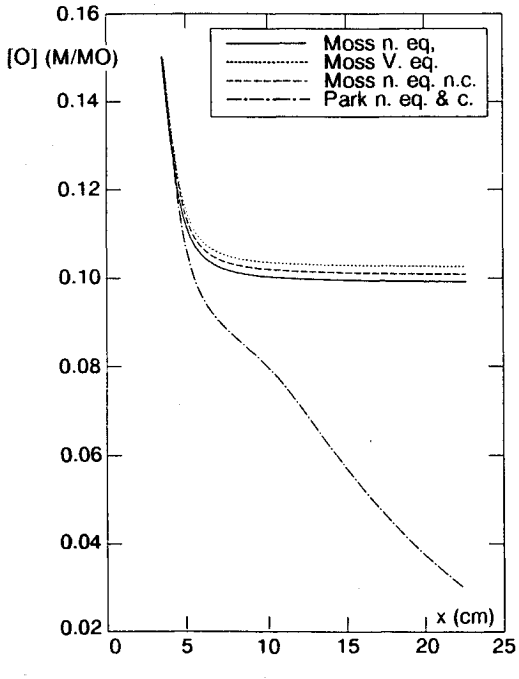

Fig. 14 Vibrational nonequilibrium and vibration-dissociation coupling effects: atomic oxygen concentration.

Comparison with Experiment

During the prototype test campaign, only measurements of stagnation enthalpy with two spherical calorimetric probes and another one measuring the surface stagnation temperature of a sphere (the flow was free of solid particles) and the frozen Mach number through a Pitot tube were performed. The measured enthalpy was different from the design enthalpy (65 instead of 100). The viscous effects were negligible[5] due to the shortness of the nozzle. Therefore, we ran a new calculation with the Moss reference model. The results are shown in Fig. 15. The discrepancy with the experiment is about 7 percent on the frozen Mach number, which is not so bad considering all the theoretical uncertainties. We would have tested more ther-

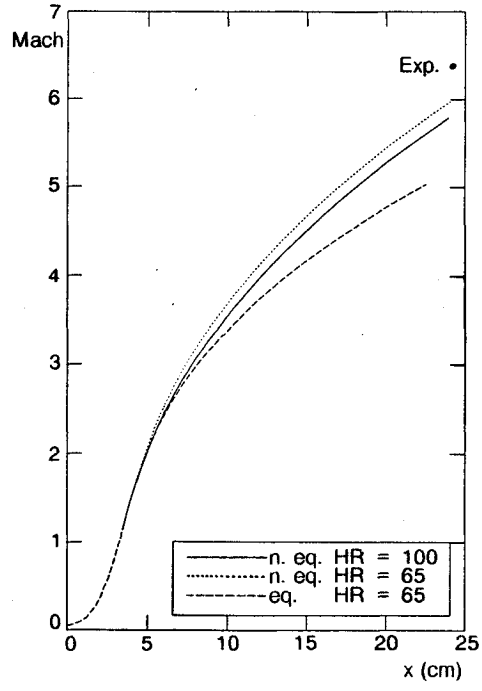

Fig. 15 Moss model: comparison of frozen Mach number with experiment.

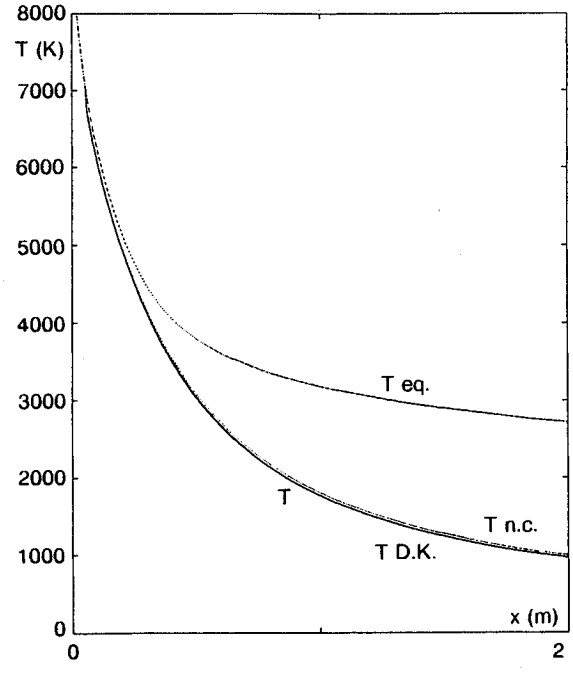

Fig. 16 High enthalpy nozzle: translational temperatures: DK., Moss, Moss without coupling, equilibrium.

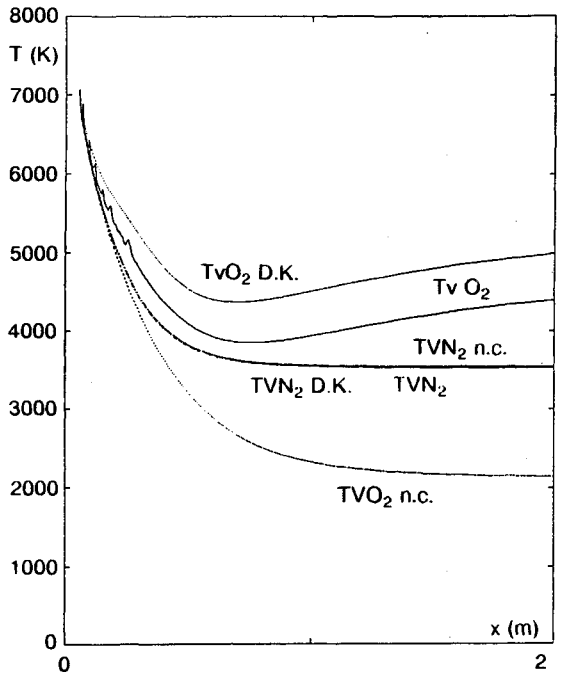

Fig. 17 High enthalpy nozzle: O2 and N2 vibrational temperatures: DK, Moss, Moss without coupling.

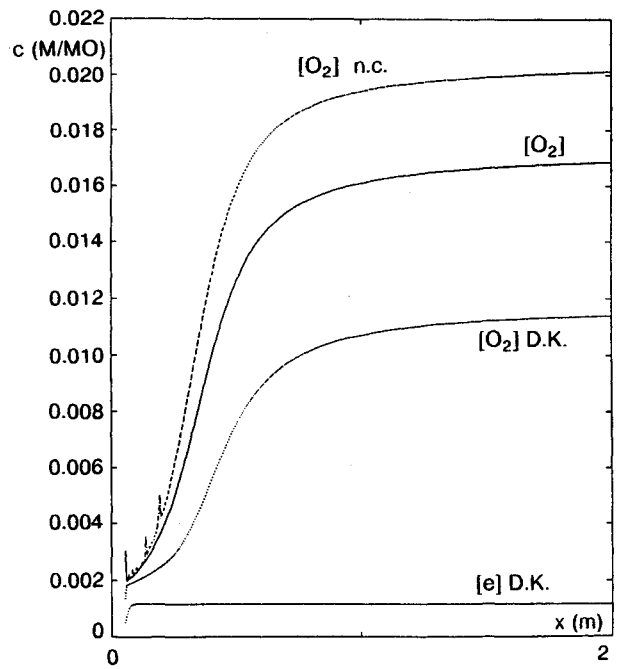

Fig. 18 High enthalpy nozzle: species concentrations: [e] DK., [O2] DK, [O2] Moss, [O2] Moss without coupling.

mochemical models and also introduced the real area variation, which is spherical instead of flat,[5] if concentrations, vibrational temperatures, velocity, or pressure measurements had been available.

Generic Wind Tunnel

The study of this nozzle is not as complete as for the first one. We are principally interested in the influence of the nonpreferential coupling. We also check the little importance of ionization (by comparison between Moss and DK chemical sets) for these stagnation conditions. Figure 16 (throat located at $x = 0$) shows the evolutions of several translational temperatures: equilibrium (Teq.), Moss nonequilibrium (T), and without coupling (Tn.c.), DK nonequilibrium (TD.K.). TD.K. and T are indistinguishable, whereas Tn.c. is very close to them and, as expected, Teq. is higher. In Fig. 17, we observe that the coupling is more important in this nozzle: taking it into account that it has a large effect on TvO2. Coupling leads to unfrozen TvO2 (Moss and DK) higher than TvN2, insensitive to chemistry or coupling. The vibrational temperature of oxygen even increases toward the nozzle exit, whereas the translational temperature keeps decreasing. Noncoupling yields a frozen TvO2 behaving in the same way as for the former nozzle, but freezing (TvO2n.c. and TvN2's) occurs more slowly and at relatively lower levels. This is due to the higher density, enabling more collisional exchanges. For the corresponding O_2 concentrations, the choice of a chemistry model is as important as coupling or no coupling (Fig. 18), and freezing does not actually occur, although the maximum exit $[O_2]$ is about 10 times less than the equilibrium value (about 0.2 for 1000 K). As expected, the DK model shows that the ionization is weak and [e] freezing occurs almost at the calculation starting point.

Conclusions

The conclusion of this study is that it is very important to correctly model the chemical vibrational nonequilibrium for these types of nozzle flows. Park coupling, in the way it has been introduced in the code, yields different solutions from the other models that were tested. The choice of chemistry and the electronic excitation have weak effects on the aerodynamics: most of the chemistry sets gave similar results despite strong differences in the species involved and in their kinetics. When it is necessary to determine accurately the gas composition at the nozzle exit, all these phenomena are important.

The vibration-dissociation nonpreferential coupling had little effect in the first nozzle study, but played an important role for the second nozzle flow: new unexpected physical phenomena appear due to its severe stagnation conditions.

Nevertheless, these conclusions apply only to these types of nozzle flows: each new problem would require a complete investigation. The quasi-one-dimensional code appears as a very useful tool, allowing the classification of thermochemical phenomena, in order to separate the flow into different zones where some simplifications are possible (equilibrium, freezing, etc.) before using more sophisticated methods. Furthermore this type of code allows numerical experiments since it is possible to easily introduce and test different thermochemical models that could be used in more general programs and to get precious information on the quality of the nozzle flow.

Appendix A: Closure Equations

In order to close the system of equations, we need the following relations:

$$Cp_j = \frac{5 + 2(n_j - 1)}{2} + (n_j - 1)\left(\frac{\theta v_j}{T}\right)^2 \frac{\exp(\theta v_j/T)}{[\exp(\theta v_j/T) - 1]^2} + \frac{\left[\sum_{i=1}^{m} G_{jl}\right]\left[\sum_{i=1}^{m} (\frac{E_{jl}}{T})^2 G_{jl}\right] - \left[\sum_{i=1}^{m} E_{jl}\, G_{jl}\right]\left[\sum_{i=1}^{m} \frac{E_{jl}}{T^2} G_{jl}\right]}{\left[\sum_{i=1}^{m} G_{jl}\right]^2} \tag{A1}$$

This is written for vibrational equilibrium. In the case of vibrational nonequilibrium, the second term of the C_{pj} is removed and the vibrational contribution is modeled by the term $d\epsilon_\alpha/dx$ in Eq. (5). The vibrational and electronic excitations also have an influence on the chemical potentials and,

Table B1 Chemical reaction rate coefficients k'^{∞}_i

	Dunn & Kang model : O, N, O_2, N_2, NO, e,NO+,O_2+,N_2+,O+,N+			E.S.H. model : O, N, O_2, N_2, NO, e, NO+			Moss model : O, N, O_2, N_2, NO			Gardiner model : O, N, O_2, N_2, NO			Park model : O, N, O_2, N_2, NO		
Dissociation reactions:	a_i	b_i	c_i	a_i	b_i	c_i	a_i	b_i	c_i	a_i	b_i	c_i	a_i	b_i	c_i
$O_2 + N \rightarrow 2O + N$	3.61 E18	-1.	.594 E5	3.61 E18	-1.	.594 E5	3.61 E18	-1.	.594 E5	1.82 E18	-1.	.5938 E5	2.90 E23	-2.	.5975 E5
$O_2 + NO \rightarrow 2O + NO$	3.61 E18	-1.	.594 E5	3.61 E18	-1.	.594 E5	3.61 E18	-1.	.594 E5	1.82 E18	-1.	.5938 E5	9.68 E22	-2.	.5975 E5
$O_2 + O_2 \rightarrow 2O + O_2$	3.249 E19	-1.	.594 E5	3.249 E19	-1.	.594 E5	3.249 E19	-1.	.594 E5	1.64E19	-1.	.5938 E5	9.68 E22	-2.	.5975 E5
$O_2 + N_2 \rightarrow 2O + N_2$	7.22 E18	-1.	.594 E5	7.22 E18	-1.	.594 E5	7.22 E18	-1.	.594 E5	3.64 E18	-1.	.5938 E5	9.68 E22	-2.	.5975 E5
$O_2 + O \rightarrow 2O + O$	9.025 E19	-1.	.594 E5	9.025 E19	-1.	.594 E5	9.025 E19	-1.	.594 E5	4.56 E19	-1.	.5938 E5	2.90 E23	-1.	.5975 E5
$N_2 + N \rightarrow 2N + N$	4.08 E22	-1.5	1.132 E5	2.1 E22	-1.5	1.132 E5	4.15 E22	-1.5	1.132 E5	1.6 E22	-1.6	1.132 E5	1.6 E22	-1.6	1.132 E5
$N_2 + NO \rightarrow 2N + NO$	1.9 E17	-.5	1.132 E5	1.92 E17	-.5	1.132 E5	1.92 E17	-.5	1.132 E5	1.4 E21	-1.6	1.132 E5	4.98 E21	-1.6	1.132 E5
$N_2 + O_2 \rightarrow 2N + O_2$	1.9 E17	-.5	1.132 E5	1.92 E17	-.5	1.132 E5	1.92 E17	-.5	1.132 E5	1.4 E21	-1.6	1.132 E5	3.7 E21	-1.6	1.132 E5
$N_2 + N_2 \rightarrow 2N + N_2$	4.70 E17	-.5	1.132 E5	4.80 E17	-.5	1.132 E5	4.80 E17	-.5	1.132 E5	3.7 E21	-1.6	1.132 E5	3.7 E21	-1.6	1.132 E5
$N_2 + O \rightarrow 2N + O$	1.92 E17	-.5	1.132 E5	1.92 E17	-.5	1.132 E5	1.92 E17	-.5	1.132 E5	1.4 E21	-1.6	1.132 E5	4.98 E22	-1.6	1.132 E5
$NO + N_2 \rightarrow N + O + N_2$	3.97 E20	-1.5	.7551 E5	3.97 E20	-1.5	.7551 E5	3.97 E20	-1.5	.7551 E5	4. E20	-1.5	.7551 E5	7.95 E23	-2.	.7551 E5
$NO + N \rightarrow N + O + N$	7.8 E20	-1.5	.7551 E5	7.94 E21	-1.5	.7551 E5	7.94 E21	-1.5	.7551 E5	8. E20	-1.5	.7551 E5	7.95 E23	-2.	.7551 E5
$NO + O_2 \rightarrow N + O + O_2$	3.97 E20	-1.5	.7551 E5	3.97 E20	-1.5	.7551 E5	3.97 E20	-1.5	.7551 E5	4. E20	-1.5	.7551 E5	7.95 E23	-2.	.7551 E5
$NO + O \rightarrow N + O + O$	7.8 E20	-1.5	.7551 E5	7.94 E21	-1.5	.7551 E5	7.94 E21	-1.5	.7551 E5	8. E20	-1.5	.7551 E5	7.95 E23	-2.	.7551 E5
$NO + NO \rightarrow N + O + NO$	7.8 E20	-1.5	.7551 E5	7.94 E21	-1.5	.7551 E5	7.94 E21	-1.5	.7551 E5	8. E20	-1.5	.7551 E5	7.95 E23	-2.	.7551 E5
Shuffle reactions															
$O + NO \rightarrow N + O_2$	3.18 E9	1.	1.968 E4	3.18 E9	1.	1.968 E4	3.18 E9	1.	1.968 E4	3.8 E9	1.	2.082 E4	8.37 E12	0.	1.945 E4
$O + N_2 \rightarrow N + NO$	7. E13	0.	3.8 E4	6.75 E13	0.	3.7755 E4	6.75 E13	0.	3.7755 E4	1.82 E14	0.	3.837 E4	6.44 E17	-1.	3.7755 E4
Ionization reactions															
$O + N \rightarrow NO^+ + e$	1.40 E6	1.5	3.19 E4	2.40 E10	0.5	3.24 E4									
$O + e \rightarrow O^+ + 2e$	3.6 E31	-2.91	1.58 E5												
$N + e \rightarrow N^+ + 2e$	1.1 E32	-3.14	1.69 E5												
$O + O \rightarrow O_2^+ + e$	1.6 E17	-.98	8.08 E4												
$O + O_2^+ \rightarrow O_2 + O^+$	2.92 E18	-1.11	2.8 E4												
$O_2 + N_2 \rightarrow NO + NO^+ + e$	1.38 E20	-1.84	1.41 E5												
$NO + N_2 \rightarrow NO^+ + N_2 + e$	2.2 E15	-.35	1.08 E5												
$O + NO^+ \rightarrow NO + O^+$	3.63 E15	-.6	5.08 E4												
$N_2 + O^+ \rightarrow O + N_2^+$	3.4 E19	-2.	2.3 E4												
$N + NO^+ \rightarrow NO + N^+$	1. E19	-.93	6.1 E4												
$O_2 + NO^+ \rightarrow NO + O_2^+$	1.8 E15	.17	3.3 E4												
$O + NO^+ \rightarrow O_2 + N^+$	1.34 E13	.31	7.727 E4												
$O_2 + NO \rightarrow NO^+ + O_2 + e$	8.8 E15	-.35	1.08 E5												
$N_2 + N^+ \rightarrow N + N_2^+$	2.02 E11	.81	1.3 E4												
$N + N \rightarrow N_2^+ + e$	1.4 E13	0.0	6.78 E4												

therefore, on chemical equilibrium. In effect, the equilbrium constants are written as

$$K'_{pi} = \exp\left[\frac{-\Delta F_i 0}{R'T'}\right], \quad K'_i = K'_{pi}\,(R'T')^{\beta i}$$

$$\text{with} \quad \frac{\Delta F_i 0}{R'T'} = \sum_{j=1}^{s} \beta_{ij} \frac{\mu_j 0}{T} \tag{A2}$$

The chemical potentials come from the partition functions:

$$\frac{\mu_j{}^0 - h_j{}^0}{T} = -\frac{3}{2}\ell n \frac{2\pi m'_j k}{h^2} - \ell n \frac{k}{P'_0} + (n_j - 1)\,\ell n\,\theta' r_j - \ell n\, g_{jl=1}$$
$$- \frac{5 + 2(n_j - 1)}{2}\ell n\, T' + (n_j - 1)\ell n\,[1 - \exp(-\theta v_j/T)]$$
$$- \ell n\left[\frac{\sum_{l=1}^{m} G_{jl}}{g_{jl=1}}\right] \tag{A3}$$

where $h_j{}^0$ is the enthalpy of formation of the jth species and p'_0 is the standard pressure.

The equilibrium vibrational energy of the harmonic oscillator writes

$$\epsilon_j{}^{\infty} = \frac{\theta v_j}{\exp(\theta v_j/T) - 1} \tag{A4}$$

In case of nonequilibrium, the vibrational temperature comes from

$$Tv_j = \frac{\theta v_j}{\ell n\,(1 + \theta v_j/\epsilon_j)} \tag{A5}$$

Appendix B

The chemical reaction rate coefficients $k'_i{}^{\infty}$ (in cm^3 $mole^{-1}$ s^{-1} for binary reactions) are in Table B1.

References

[1]Consigny, H., Pacou, C., Papirnik, O., Sagnier, Ph., and Chevallier, J.P., "Préparation d'essais Probatoires d' un Générateur de Plasma Pour l'Alimentation d'une Soufflerie Hypersonique," AGARD CP 428, April 1987.

[2]Pacou, C., "Analyse des Moyens d'essais Nécessaires à l'etude des Problèmes de Rentrée. Avant Projet d'un Moyen d'essais Hypersonique à Haute Enthalpie (Soufflerie R6Ch) pour le programme HERMES," Office National d'Etudes et de Recherches Aérospatiales 95/1865 AH, Feb. 1986.

[3]Marrone, P. V., Hall, J. G., and Garr L. J., "Inviscid, Non Equilibrium Flow Behind Bow and Normal Shock Waves," CAL Rep. QM 1626 A12 (Part I and II), May 1963.

[4]Bouniol, F., "COURLI: Programme de calcul d'un Ecoulement Hors Equilibre le Long d'une Ligne de Courant," Office National d'Etudes et de Recherches Aéospatiales 4/1229 AN, July 1969.

[5]Sagnier, Ph., "Ecoulement Horse Equilibre dans la tuyére Probatoire R6 pour les Conditions Nominales de Founctionnement," Office National d'Etudes et de Recherches Aérospatiales 95/1865 AH, July 1986.

[6]Sagnier, Ph., "Programme de Calcul de l'écoulement non Visqueux d'un Gaz réel Dans une Tuyére de Soufflerie Hypersonique," Office National d'Etudes et de Recherches Aérospatiales 100/1865 AN, Sept. 1987.

[7]Landau, L., and Teller, E., "Zur Theorie der Schalldispersion," *Physic Z. Sowjetunion*, 1936.

[8]Blackman, V.H., "Vibrational Relaxation in Oxygen and Nitrogen," *Journal of Fluid Mechanics*, Vol. 1, 1956, pp. 61, 85.

[9]Park, C., "Assessment of Two Temperature Kinetic Model for Dissociating and Weakly Ionizing Nitrogen," AIAA Paper 86-1347, June 1986.

[10]Park, C., "Assessment of Two Temperature Kinetic Model for Ionizing Air," AIAA Paper 87-1574, June 1987.

[11]Marraffa, L., Dulikravich, G. S., Keeney, T. C., and Deiwert G. S., "A survey of the Reaction Rate Constants for the Thermal Dissociation and Recombination of Nitrogen and Oxygen," AIAA Paper 88-0754, Jan. 1988.

[12]Brun, R., Colas, P., Gubernatis, P., Zeitoun D., "Practical Physico-Chemical Models for High Speed Air Flow-Field Computations," *Journal of Thermophysics of Fluids* (to be published).

[13]Miner, E. W., and Lewis C. H., "Hypersonic Ionizing Air Viscous Shock Layer Flows over Nonanalytic Blunt Bodies," NASA CR-2550, May 1975.

[14]Aupoix, B., and Eldem, C., "Couches Limites Hypersoniques an Equilibre ou Déséquilibre Chimique," Office National d'Etudes et de Recherches Aérospatiales CERT-DERAT 15/5005 DY, Jan. 1987.

[15]Aupoix, B., Arnal, D., and Eldem C., "Problémes de Couche Limite liés au Projet Hermés", 24° Colloque AAAF, Poitiers, Oct. 1987.

[16]Eldem, C., "Couches Limites Hypersoniques avec Effets de Dissociation," Thèse de Doctorat de l'ENSAE, Toulouse, Dec. 1987.

[17]Shinn, J. L., Moss, J. N., and Simmonds A. L., "Viscous Shock Layer Heating Analysis for the Shuttle Winward Plane with Surface Finite Catalytic Recombination Rates," AIAA Paper 82-0842, June 1982.

[18]Gardiner, W. C., Jr, *Combustion Chemistry,* Springer-Verlag, Berlin 1984.

[19]Evans, J. S., Schexnayder, C. J., Jr, and Huber, P. W., "Boundary Layer Electron Profiles for Entry of a Blunt Slender Body at High Altitudes," NASA TND-7332, June 1973.

[20]Dunn, M. G., and Kang, S. W., "Theoretical and Experimental Studies of Re-entry Plasmas," NASA CR-2232, April 1973.

[21]Hilsenrath, J., and Klein, M., "Tables of Thermodynamic Properties of Air in Chemical Equilibrium Including Second Virial Correction from 1500 K to 15000 K," Arnold Engineering Development Center, TR-65-58, March 1965.